2. DEVELOPMENT OF AN EXPLICIT TIME MARCHING PROCEDURE

FOR LAMINAR AND TURBULENT FLOW

- SUMMARY VIEWGRAPHS

AN EXPLICIT FINITE-VOLUME TIME-MARCHING PROCEDURE
FOR TURBULENT FLOW CALCULATIONS

Start: Denton explicit time-marching method.
Allure – easy to understand method.

Continuity

$$\frac{\partial \rho}{\partial t} + \frac{\partial \rho u}{\partial x} + \frac{\partial \rho v}{\partial y} + \frac{\partial \rho w}{\partial z} = 0$$

$$\delta \rho = \left[- \frac{\partial \rho u}{\partial x} - \frac{\partial \rho v}{\partial y} - \frac{\partial \rho w}{\partial z} \right] \delta t$$

Momentum

$$\delta(\rho u) = [\text{steady eqn momentum error}] \, \delta t$$

$$\delta(\rho v) = [\qquad\qquad\qquad\qquad] \, \delta t$$

$$\delta(\rho w) = [\qquad\qquad\qquad\qquad] \, \delta t$$

Start: Denton explicit time-marching method.

Questions:

1. Is smoothing necessary for convergence of explicit method ?

2. Why, at low Mach numbers, is the CFL criterion used to get the
   time step for the momentum equations ?
   $$(\delta t = \delta x/[\text{velocity} + \text{speed of sound}])$$

3. Why not extend the method to laminar and turbulent flow ?
       What are the problems involved ?

4. Why does he use an interpolated pressure in the momentum
   equation for transonic flow ?
       Can we show why and when it is stable ?

5. How can the method be extended to separated flow ?

ANSWER   ------->

Development of Explicit method for calculation of
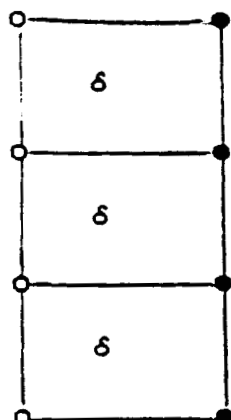
Inviscid, Laminar or Turbulent Flow

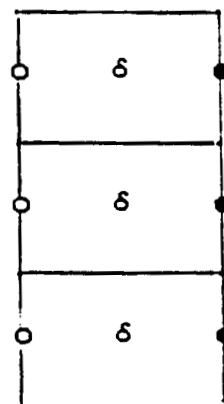Mach number = 0 to >2.5, including shocks

Economical - grid points

With or without separation

Tested on 2-d duct flows

1. Is smoothing necessary for convergence of explicit method ?

Denton control volume
   4 unknowns   ●
   3 equations

     YES

FLOW

------>

"New" control volume
     3 unknowns   ●
   3 (well-posed) equations

      NO

("New" control volume, traditionally used for boundary layers)

2. Why, at low Mach numbers, is the CFL criterion used
   to get the time step for the momentum equations ?
        ($\delta t = \delta x / [\text{velocity} + \text{speed of sound}]$)

CONSERVATIVE FORM OF MOMENTUM EQUATION

$$\frac{\partial(\rho u)}{\partial t} + \nabla \cdot \rho \underline{u}\, u = -\frac{\partial p}{\partial x} + \ldots$$

$$u \left[\frac{\partial \rho}{\partial t} + \nabla \cdot \rho \underline{u} \right] + \rho \frac{\partial u}{\partial t} + \rho \underline{u} \cdot \nabla u = -\frac{\partial p}{\partial x} + \ldots$$

   continuity

  included, therefore $\delta t_{cont} = \delta t_{mom}$
  Stability analysis, continuity and momentum --->

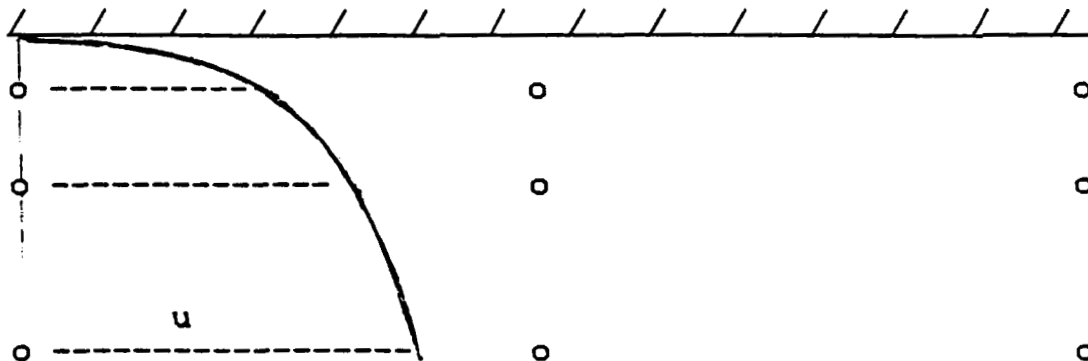 CFL condition $\delta t = \delta x/(u+c)$

CONVECTIVE FORM OF EQUATION

$$\rho \frac{\partial u}{\partial t} + \rho \underline{u} \cdot \nabla u = -\frac{\partial p}{\partial x} + \ldots$$

Stability analysis, momentum equation ---> $\delta t = \delta x/u$

3. Why not extend the method to laminar and turbulent flow ?
   What are the problems involved ?

RESOLUTION OF TRANSVERSE PRESSURE GRADIENT

Flat plate turbulent boundary layer $\partial p/\partial y \simeq 0$

$$p = \rho RT$$

$$\delta p = RT\, \delta\rho - \frac{\rho RU\, \delta U}{2c_p}$$

δp dependent on continuity and momentum errors –
        stability is highly grid and δt dependent
        difficult without smoothing

Borrow idea from pressure correction methods –
        δp depends only on continuity error.

$$\delta p = RT\, \delta\rho$$

$$= [\; -\frac{\partial\rho u}{\partial x} - \frac{\partial\rho v}{\partial y} - \frac{\partial\rho w}{\partial z}\;]\; RT\, \delta t$$

Stable without smoothing. Multi-volume approach
needed for highly nonuniform δy grid spacing.

4. Why does Denton use an interpolated pressure in
   the momentum equation for transonic flow ?
        Can we show why and when it is stable ?

   Want $\dfrac{\partial \rho u}{\partial x} + \dfrac{\partial \rho v}{\partial y} + \dfrac{\partial \rho w}{\partial z} = 0$

   1-D stability analysis. $\rho = \rho + \delta\rho$
                                $u = u + \delta u$
                                $\delta u \simeq - C\, \partial(\delta p)/\partial x$
                                $\delta p \simeq RT\, \partial\rho$
   Interpolated pressure

   $p_i = (\rho RT)_i$ or $p_i = .5[(\rho RT)_{i+1} + (\rho RT)_{i-1}]$ or ...

   $----->$
   $A_i \delta\rho_i + A_{i+1}\delta\rho_{i+1} + A_{i-1}\delta\rho_{i-1} + ...$
             $=$ continuity error, each control volume

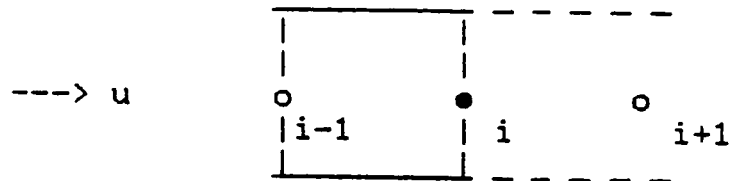   Explicit method approximation
   $[1/\delta t]\ \delta\rho_i =$ continuity error for control volume

   Stability requires A_i positive and dominant.

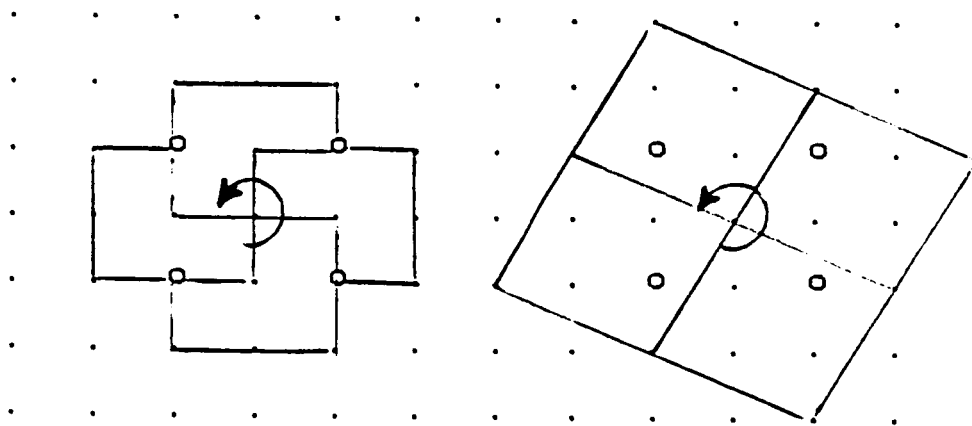## 5. How can the method be extended to separated flow ?

(a) UPWIND DIFFERENCING

---> u

$$u > 0 \qquad u\, \partial u/\partial x = \quad u\,(u_i - u_{i-1})/\delta x$$

$$u < 0 \qquad u\, \partial u/\partial x = (-u)(u_i - u_{i+1})/\delta x$$

---> positive coefficient for u_i

(b) UPWINDED CONTROL VOLUMES
- control volumes depend on local $\underline{u}$

---> positive coefficient for u_i
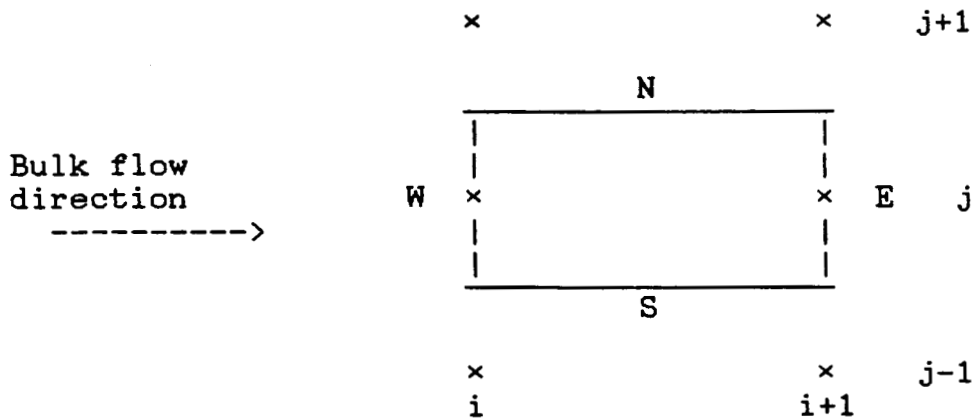
3. LIST OF PROJECT REPORTS AND PAPERS

1. Nicholson, S., "Development of a Finite Volume Time Marching Method," Turbomachinery Research Group Report No. JM/85-3, Mechanical Engineering Dept., VPI&SU, February 1985.

2. Nicholson, S., and Moore, J., "Semi-Annual Status Report on NASA Grant No. NAG 3-593 for the Period 12/20/84 - 5/31/85," Turbomachinery Research Group Report No. JM/85-6, Mechanical Engineering Dept., VPI&SU, June 1985.

3. Moore, J., Nicholson, S., and Moore, J.G., "Annual Report on NASA Grant No. NAG 3-593 for the Period 12/20/84 - 12/19/85," Turbomachinery Research Group Report No. JM/85-11, Mechanical Engineering Dept., VPI&SU, December 1985.

4. Nicholson, S., and Moore, J., "Semi-Annual Status Report on NASA Grant No. NAG 3-593 for the Period 12/20/85 - 5/31/86," Turbomachinery Research Group Report No. JM/86-2, Mechanical Engineering Dept., VPI&SU, June 1986.

5. Nicholson, S., "Extension of the Finite Volume Method to Laminar and Turbulent Flow," Ph. D. Dissertation and Turbomachinery Research Group Report No. JM/86-6, Mechanical Engineering Dept., VPI&SU, August 1986.

6. Nicholson, S., Moore, J.G., and Moore, J., "An Explicit Finite-Volume Time-Marching Procedure for Turbulent Flow Calculations," 5th International Conference on Numerical Methods in Laminar and Turbulent Flow, Montreal, Canada, July, 1987.

7. Nicholson, S., Moore, J.G., and Moore, J., "Explicit Finite-Volume Time-Marching Calculations of Total Temperature Distributions in Turbulent Flow," 5th International Conference on Numerical Methods in Laminar and Turbulent Flow, Montreal, Canada, July, 1987.

4. BACKFLOW - EXTENSIONS TO THE COMPUTATIONAL PROCEDURE

4a. Discretization of Convection Terms

The momentum and energy equations are discretized over control volumes fixed relative to the grid points. Central differencing is used except in regions where there are large cross flows or backflow. In these regions a side upwind or reverse upwind differencing is used for stability. The details are as follows.

Control volume for momentum or energy for point i+1,j.

```
                     ×                       ×       j+1
                                  N
                          ┌──────────────────┐
    Bulk flow             │                  │
    direction        W  × │                  │ ×   E    j
    ----------->          │                  │
                          └──────────────────┘
                                  S
                     ×                       ×       j-1
                     i                      i+1
```

Convection of property ϕ where
ϕ = u for x-momentum
ϕ = v for y-momentum
ϕ = h for energy (enthalpy) equation.

Convection term integrated over control volume

$$\int \rho \underline{u} \cdot \nabla \phi \, dVol = \int \nabla \cdot \rho \underline{u} \phi \, dVol - \phi_M \int \nabla \cdot \rho \underline{u} \, dVol$$

$$= \oint \phi \rho \underline{u} \cdot d\underline{A} - \phi_M \oint \rho \underline{u} \cdot d\underline{A}$$

$$= (\rho \underline{u} \cdot \underline{A})_N \phi_N + (\rho \underline{u} \cdot \underline{A})_S \phi_S + (\rho \underline{u} \cdot \underline{A})_E \phi_E + (\rho \underline{u} \cdot \underline{A})_W \phi_W$$

$$- \phi_M [(\rho \underline{u} \cdot \underline{A})_N + (\rho \underline{u} \cdot \underline{A})_S + (\rho \underline{u} \cdot \underline{A})_E + (\rho \underline{u} \cdot \underline{A})_W]$$

We wish to express this in terms of the ϕ's at the grid points, i.e we want the equation in the form

$$\int \rho \underline{u} \cdot \nabla \phi \, dVol = C_E \phi_{i+1,j} + C_W \phi_{i,j} + C_{EE} \phi_{i+2,j}$$

$$+ C_{NE} \phi_{i+1,j+1} + C_{NW} \phi_{i,j+1} + C_{SE} \phi_{i+1,j-1} + C_{SW} \phi_{i,j-1}$$

The coefficients C are determined from the mass fluxes through the sides ($\rho\underline{u}\cdot\underline{A}$) and the discretization choice for ϕ_N, ϕ_S, ϕ_E, ϕ_W, and ϕ_M.

For stability we wish the center point coefficient, C_E, to be positive and greater than the sum of the other positive coefficients.

$$\underline{\phi_M}$$

When $[(\rho\underline{u}\cdot\underline{A})_N+(\rho\underline{u}\cdot\underline{A})_S+(\rho\underline{u}\cdot\underline{A})_E+(\rho\underline{u}\cdot\underline{A})_W] > 0$

take $\phi_M = \phi_{i,j}$

to give a negative contribution to C_W.

When $[(\rho\underline{u}\cdot\underline{A})_N+(\rho\underline{u}\cdot\underline{A})_S+(\rho\underline{u}\cdot\underline{A})_E+(\rho\underline{u}\cdot\underline{A})_W] < 0$

take $\phi_M = \phi_{i+1,j}$

to give a positive contribution to C_E.

$$\underline{\phi_E \text{ and } \phi_W}$$

When $(\rho\underline{u}\cdot\underline{A})_E > 0$

$\phi_E = \phi_{i+1,j}$

This centered evaluation of ϕ_E (second order accurate) gives a positive contribution to C_E.

When $(\rho\underline{u}\cdot\underline{A})_E < 0$

$\phi_E = \phi_{i+2,j}$

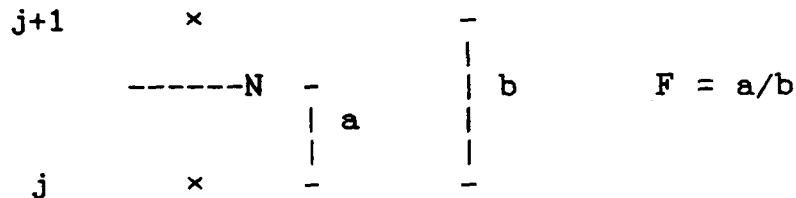This upwind evaluation of ϕ_E (first order accurate) gives a negative contribution to C_{EE}.

This also determines ϕ_W since ϕ_E for one control volume is ϕ_W for the next control volume.

ϕ_N and ϕ_S

The geometrical centered evaluation for ϕ_N is

$$\phi_N = 0.5\,[(1-F)(\phi_{i+1,j}+\phi_{i,j}) + F(\phi_{i+1,j+1}+\phi_{i,j+1})]$$

where F is the fraction of the distance of the North face between the grid points.

```
j+1        ×                 -
                             |
        ------N  -           | b        F = a/b
                 | a         |
                 |           |
   j       ×     -           -
```

For accuracy this centered evaluation should be used whenever possible.

For stability when

$$(\rho\underline{u}\cdot\underline{A})_N > 0 \text{ and } (\rho\underline{u}\cdot\underline{A})_E > 0$$

take $\qquad F \le (\rho\underline{u}\cdot\underline{A})_E/(\rho\underline{u}\cdot\underline{A})_N$

When the inequality is chosen, which for equal grid spacing will occur when $(\rho\underline{u}\cdot\underline{A})_N > 2(\rho\underline{u}\cdot\underline{A})_E$,

$$(\rho\underline{u}\cdot\underline{A})_N\phi_N = 0.5(\phi_{i+1,j} + \phi_{i,j})[(\rho\underline{u}\cdot\underline{A})_N - (\rho\underline{u}\cdot\underline{A})_E]$$

$$+ 0.5(\phi_{i+1,j+1} + \phi_{i,j+1})(\rho\underline{u}\cdot\underline{A})_E$$

When $\qquad (\rho\underline{u}\cdot\underline{A})_N > 0 \text{ and } (\rho\underline{u}\cdot\underline{A})_E \le 0$

(the primary flow is locally backwards or zero relative to the bulk flow direction)

take $\qquad \phi_N = \phi_{i+1,j}$

By symmetry for $\quad (\rho\underline{u}\cdot\underline{A})_S > 0 \text{ and } (\rho\underline{u}\cdot\underline{A})_E > 0$

take $\qquad F \ge 1 - (\rho\underline{u}\cdot\underline{A})_E/(\rho\underline{u}\cdot\underline{A})_S$

and $\qquad \phi_S = 0.5[(1-F)(\phi_{i+1,j-1}+\phi_{i,j-1}) + F(\phi_{i+1,j}+\phi_{i,j})]$

For $(\rho\underline{u}\cdot\underline{A})_S > 0 \text{ and } (\rho\underline{u}\cdot\underline{A})_E \le 0$

take $\qquad \phi_S = \phi_{i+1,j}.$

When $(\rho\underline{u}\cdot\underline{A})_N$ is negative, $(\rho\underline{u}\cdot\underline{A})_S$ is positive for the next, the j+1, control volume, so that ϕ_N is determined from ϕ_S for the j+1 control volume. Similarly when $(\rho\underline{u}\cdot\underline{A})_S$ is negative, ϕ_S is determined from ϕ_N for the j-1 control volume.

Comparison with earlier scheme.

In these terms, Nicholson (Section 3, Report 5, JM/86-6) considered only positive values for $(\rho\underline{u}\cdot\underline{A})_E$, i.e. no reverse flow. The formulae he used for ϕ_M, ϕ_E and ϕ_W were the same as given here. However the upwinding he took for the cross flows was different. In particular when $(\rho\underline{u}\cdot\underline{A})_N$ was positive, ϕ_N was evaluated using

$$F \leq \frac{1}{3} \, (\rho\underline{u}\cdot\underline{A})_{E(\text{at } i-1)} / (\rho\underline{u}\cdot\underline{A})_N + \frac{1}{3}$$

Taking $F \leq (\rho\underline{u}\cdot\underline{A})_E / (\rho\underline{u}\cdot\underline{A})_N$ gives lower and hence more conservative values of F when $(\rho\underline{u}\cdot\underline{A})_N > 2(\rho\underline{u}\cdot\underline{A})_E$, i.e., where for uniform grid spacing, the geometric F may not be used.
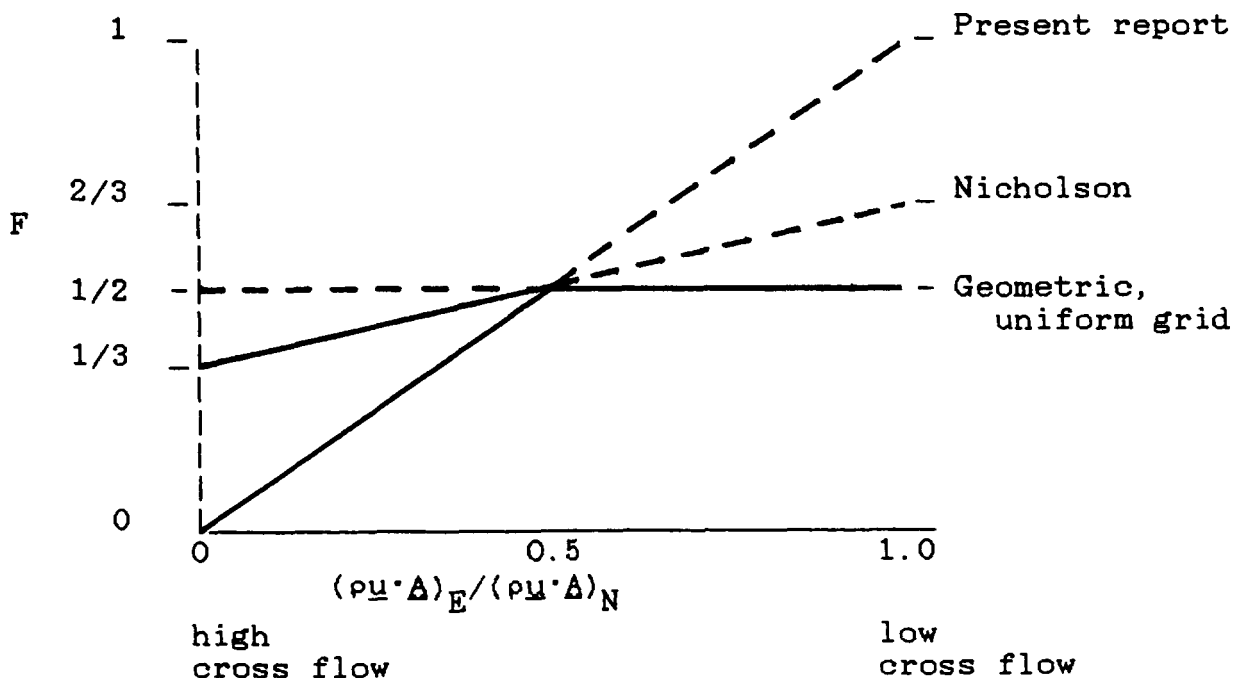
F used in calculations.

-17-

Table 1   SIDE UPWINDING ALGORITHM –
Summary for Uniform Grid Spacing

For side ▬▬, convected property = average of points marked ●.

Interpolate

Interpolate

$$E < 0 \qquad N > 0$$

$$\frac{E}{N} = 0$$

$$\frac{E}{N} > \frac{1}{2}$$

$$\frac{E}{S} > \frac{1}{2}$$

$$\frac{E}{S} = 0$$

$$E < 0 \qquad S > 0$$
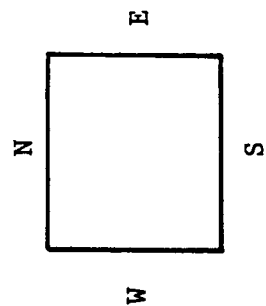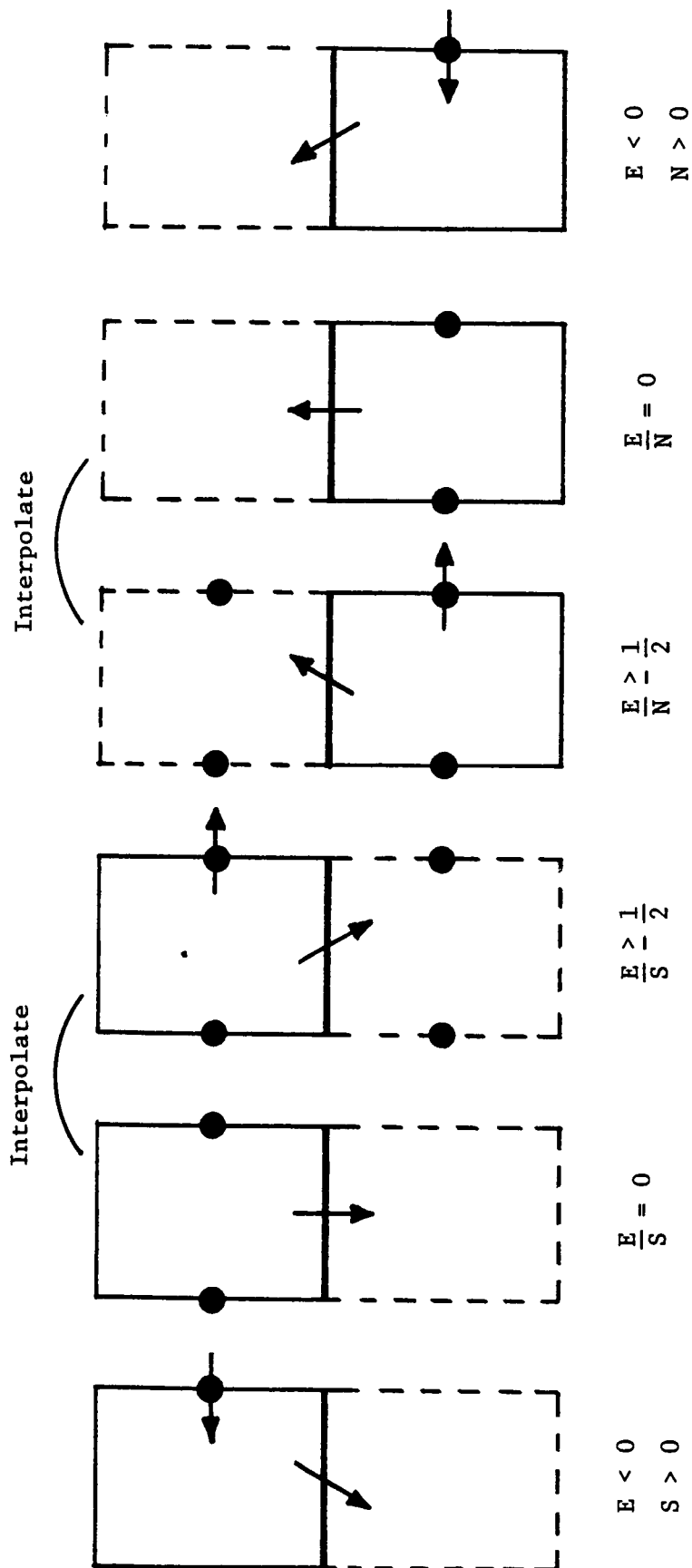
⬆ Bulk flow direction

Mass fluxes: N, S, E, W

N
W   E
S

4b. Improved Pressure Interpolation for SBLI

The same Mach number dependent pressure interpolation formula for the calculation of the density used earlier is also used here. However to converge calculations with strong shock boundary layer interactions, i.e. with shock induced separations, the Mach number used in the formula needed to be changed from the local Mach number to the local free stream Mach number. Since stability is compromised if the Mach number is underestimated but not if it is overestimated, for simplicity, the value used was the largest Mach number on the relevant pair of i-surfaces.

M_{max} for these points
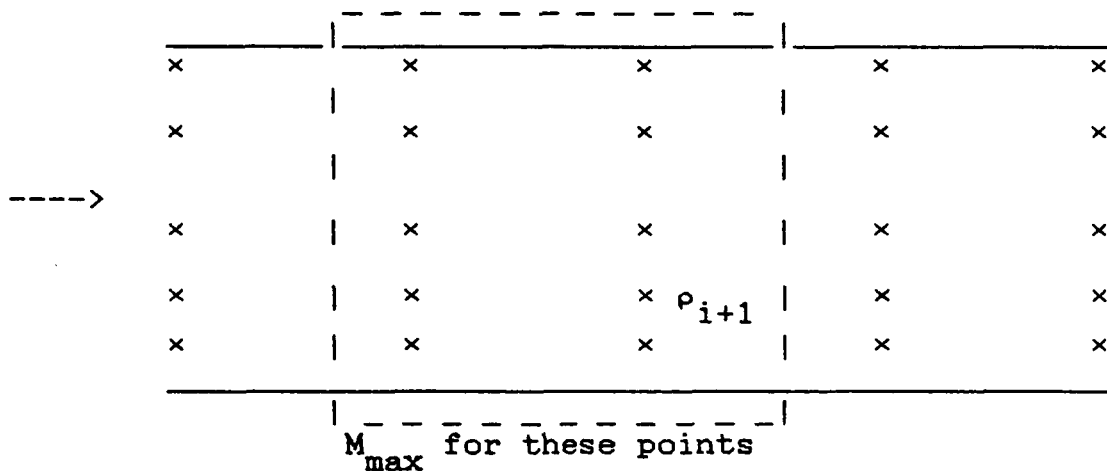
$$\rho_{i+1} = \frac{1}{RT} \left[p_i + a_0(p_{i+1} - p_i) + \frac{a_1}{2}(p_{i+1} - p_{i-1}) + \frac{a_2}{3}(p_{i+1} - p_{i-2}) \right]$$

$$a_0(M) + a_1(M) + a_2(M) = 1$$

M = Mach number = maximum Mach number at planes i and i+1.

4c. Evaluation of Turbulent Viscosity for the Present Test Cases

The turbulence model used in the calculations is a Prandtl mixing length formulation

$$\mu_t = \rho L^2 \text{``} du/dy \text{''}$$

where the mixing length L is the smaller of

       0.41y (with a Van Driest correction)
   or 0.08δ.

Sometimes it is difficult to determine an appropriate boundary layer thickness, δ.

For the present test cases

(a) UTRC, boundary layer separation geometrically triggered and
(b) Sajben diffuser, separation induced by shock,

the boundary layer thickness used to calculate L was changed to obtain a reasonable separation when compared with the measurements. The details of what was used to determine the effective boundary layer thickness follow.

Determining the edge of the boundary layer.

The location of the edge of the boundary layer is determined by the total pressure gradient $|dp_t/dy|$. In particular a search starts from outside the boundary layer (in the middle of the duct) and proceeds towards the wall to locate where

$$\left| \frac{dp_t}{dy} \right| = \frac{(p_o - p) * DPFACT}{(local\ duct\ width)} .$$

This is the edge of the boundary layer for the mixing length calculation. The larger the DPFACT the smaller the boundary layer thickness.

Case	DPFACT
(a) UTRC, sep. b.l.	2.0
(b) Sajben, $p_e/p_o = 0.722$	2.5

"Time" lag for boundary layer thickness.

For case (b), Sajben p_e/p_o = 0.722, shrinking δ by increasing DPFACT was insufficient to correctly obtain the separation induced by the shock. Qualitatively since turbulence is convected with the flow there needs to be time for the turbulence to change - it does not change suddenly. This was qualitatively introduced into the calculation by lagging the boundary layer thickness used for the calculation of L by 5 grid points. (The lag is between 0.5 and 0.75 throat heights through the separation region.) In particular after i = 40 (x/h=1.7, upstream of the shock at x/h$\simeq$2.4 but well downstream of the throat at x/h=0) the mixing length in the outer part of the boundary layer was obtained using

$$L(i) = 0.08\delta(i-5).$$

The time lag was used only for case (b).

5. BACKFLOW - TEST CASES

The extensions to the computational procedure described in section 4 were necessary for modelling two extreme cases of separated flow, the UTRC separated and reattached flat plate turbulent boundary layer (NASA Contract NAS3-22770, reference 1) and the MDRL transonic diffuser flow with a strong shock (MDRL Report No. 81-07, reference 2). These cases exhibit large boundary layer blockage (displacement thickness/local duct height), large backflow velocities, relative to the free stream velocity, and high rms/mean turbulence levels in the backflow region. The maximum boundary layer blockages were 58 percent (fifty eight!) in the UTRC low speed (U_{ref} = 27 m/s) flow and 27 percent in the MDRL diffuser with a shock Mach number of 1.353. The maximum backflow velocities were 37 percent and 25 percent, respectively, of the local maximum free-stream velocity. The ratios of rms/mean axial velocities at the locations of maximum reverse flow velocity were 35 percent in the UTRC flow and 66 percent in the MDRL diffuser. If the backflows in the two cases were varying sinusoidally, these values would correspond to maximum backflow velocities of -5.4 ± 2.7 m/s amd -71.7 ± 67.3 m/s, respectively.

UTRC Separated and Reattached Turbulent Boundary Layer

The geometry and streamlines for flow through the UTRC test section are shown in Fig. 1; and laser doppler velocity measurements are shown in Fig. 2. The corresponding calculated velocity vectors together with the locus of points for which U=0 are seen in Fig. 3. The size of the reverse flow region is well modelled, and the maximum calculated reverse flow velocity of -4.1 m/s agrees well with the measured maximum value of -5.4 m/s. This good agreement for the reverse flow leads to reasonable agreement between the measured and calculated values of skin friction coefficient in the separation zone, as shown in Fig. 4. The calculated locations of separation and reattachment are seen to be close to the measured locations. The good agreement in the separated flow region was obtained with the Prandtl mixing length model by reducing the turbulent viscosity in the boundary layer as discussed in section 4 (i.e. by using DPFACT = 2.0). This then gave a corresponding decrease in the calculated skin friction upstream and downstream of the separation zone, as seen in Fig. 4. We conclude that the present explicit computational procedure can be used for flows with extensive and strong backflow but that a more sophisticated turbulence model is required.

MDRL Diffuser - Strong Shock Case

With a back pressure, $P_{exit}/P_{o,inlet}$, of 0.722, the MDRL diffuser
G had a shock Mach number of 1.353. Shock induced separation
occurred in the turbulent boundary layer on the curved top wall.
This contrasts with the case of 0.805 pressure ratio which gave a
shock Mach number of 1.235 and no separation. In this section,
results of calculations for these two flows will be compared, with
particular attention being given to the backflow in the strong
shock case.

The calculated shock locations are clearly seen for the two
cases in the contours of static pressure in Fig. 5. The strong
shock is located further downstream and shows evidence of a lambda
foot at the curved top wall. The computed shocks are both quite
sharp as a result of the use of the M&M pressure interpolation
formula (see section 3 of this report, reference 3).

For the strong shock case, the computed and measured static
pressure distributions on the top wall are compared in Fig. 6. The
computed shock is just downstream of the measured lcoation and is
therefore somewhat stronger with a shock Mach number of 1.39.
Upstream of the shock the static pressures are indistinguishable;
but downstream the calculated static pressures are consistently
higher than those measured, perhaps partly because of
three-dimensionality in the measured flow.

The Mach number contours in Fig. 7 show the flow accelerating
up to the shock and decelerating downstream. The top wall boundary
layer thickens appreciably more through the strong shock. This is
seen also in the velocity vectors of Fig. 8, which show the
separation bubble downstream of the strong shock. Fig. 9 shows
this calculated backflow in more detail, and for comparison the
magnitude and possible variations of the measured backflow are
also shown. The maximum calculated backflow velocity of -87.7 m/s
agrees quite well with the maximum measured value of -71.7 m/s.

Figures 8 and 9 demonstrate quite graphically the significant
blockage caused by the separation bubble; and this is also seen in
Fig. 10, which shows contours of total pressure.

We conclude that calculations of diffuser flows with strong
shocks and shock induced separation can be performed with the
present explicit method. As discussed in section 4, this
calculation required a time lag of the turbulent viscosity to give
a reduced viscosity in the separation bubble. In fact, this simple
modification to the turbulence model produced a dramatic upstream
movement of the shock and the calculation rapidly converged on a
shock location close to that measured. Again this suggests the
need for a more sophisticated turbulence model. But the present
study of strong backflows has clearly demonstrated that they can

be modelled with an explicit method based on the finite volume approach.

References

1. Patrick, W.P., "Flowfield Measurements in a Separated and Reattached Flat Plate Turbulent Boundary Layer," NASA Contract No. NAS3-22770, Draft Final Report, August 1985.

2. Salmon, J.T., Bogar, T.J., and Sajben, M., "Laser Velocimeter Measurements in Unsteady, Separated, Transonic Diffuser Flows," AIAA Paper No. 81-1197 (1981). Accepted for publication in AIAA Journal.
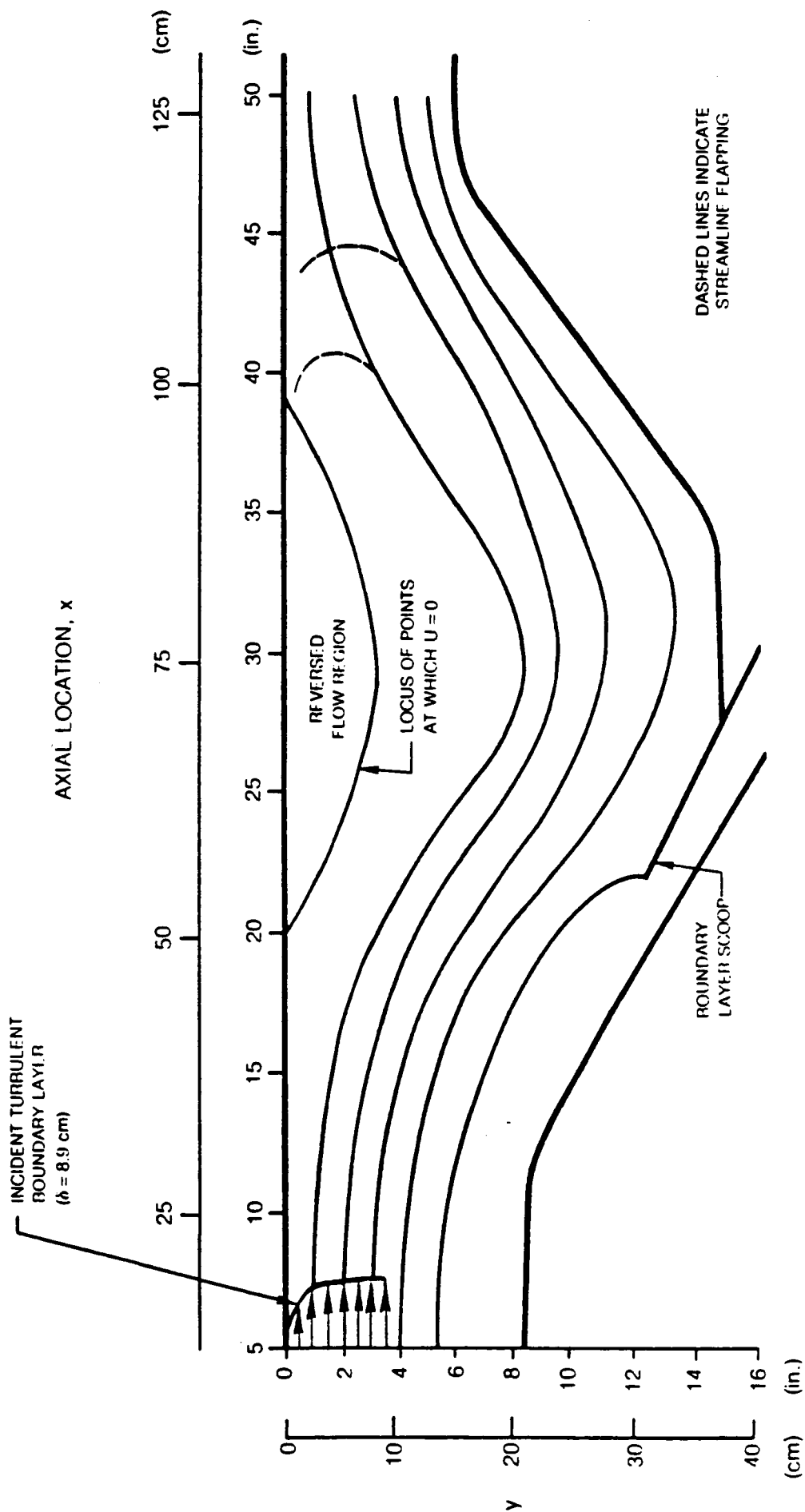
Fig. 1 Streamlines Determined from Smoke Flow Visualization and Tuft Trees (after Patrick [1])
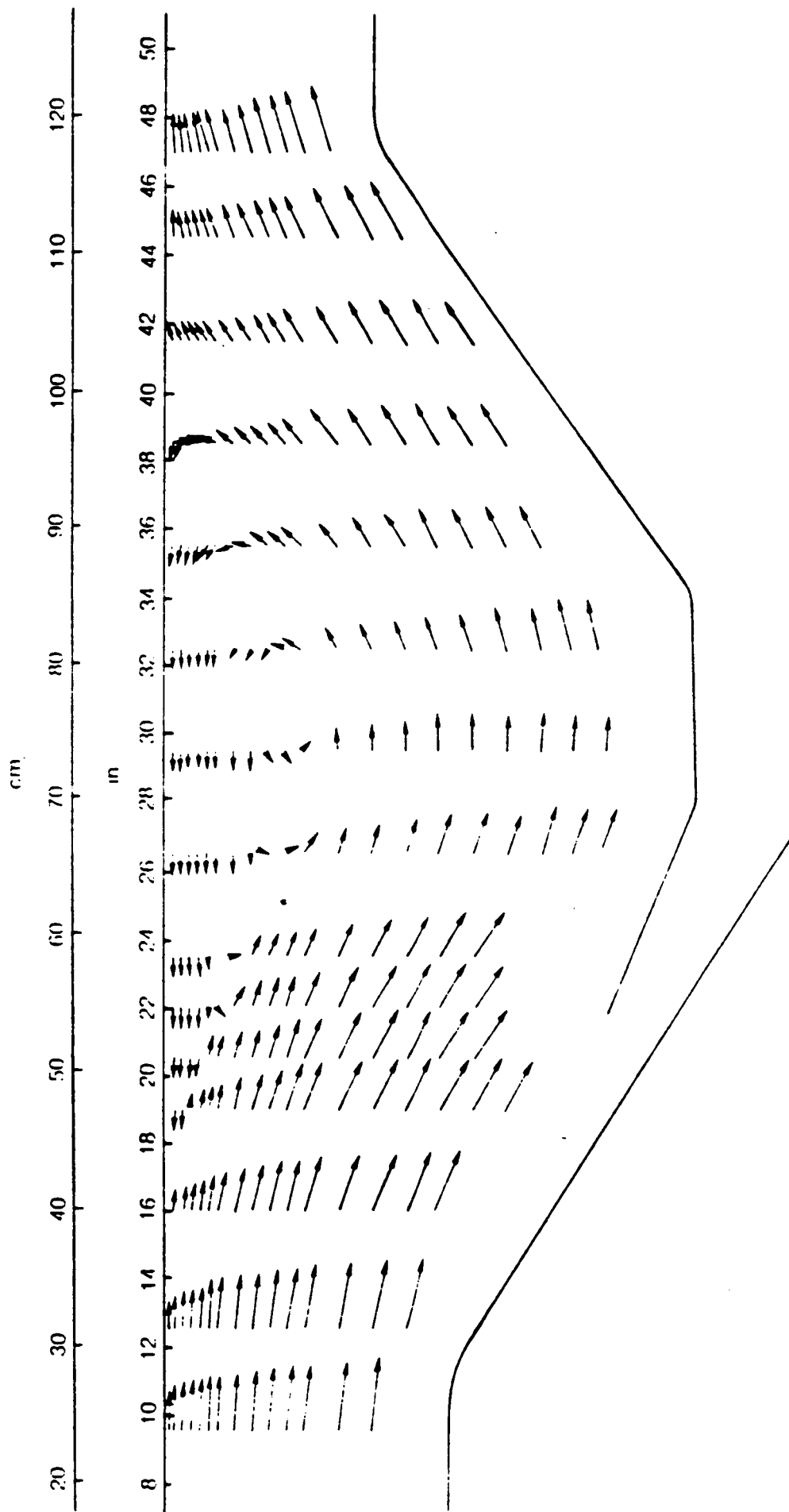
Fig. 2   LV Mean Velocity Measurements on Wind Tunnel Centerline (after Patrick [1])

UTRC SEP. B.L.
U=0

UTRC SEP. B.L.
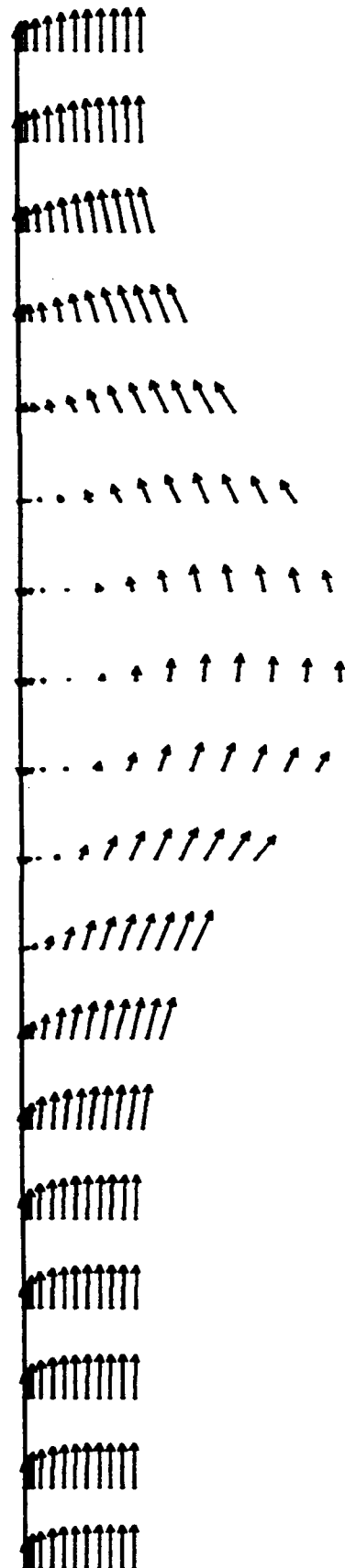
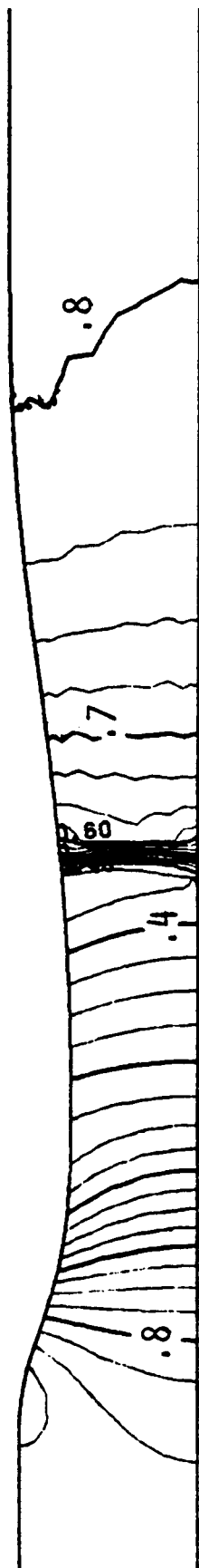Fig. 3   Calculated velocity vectors and the locus of points for which U = 0.
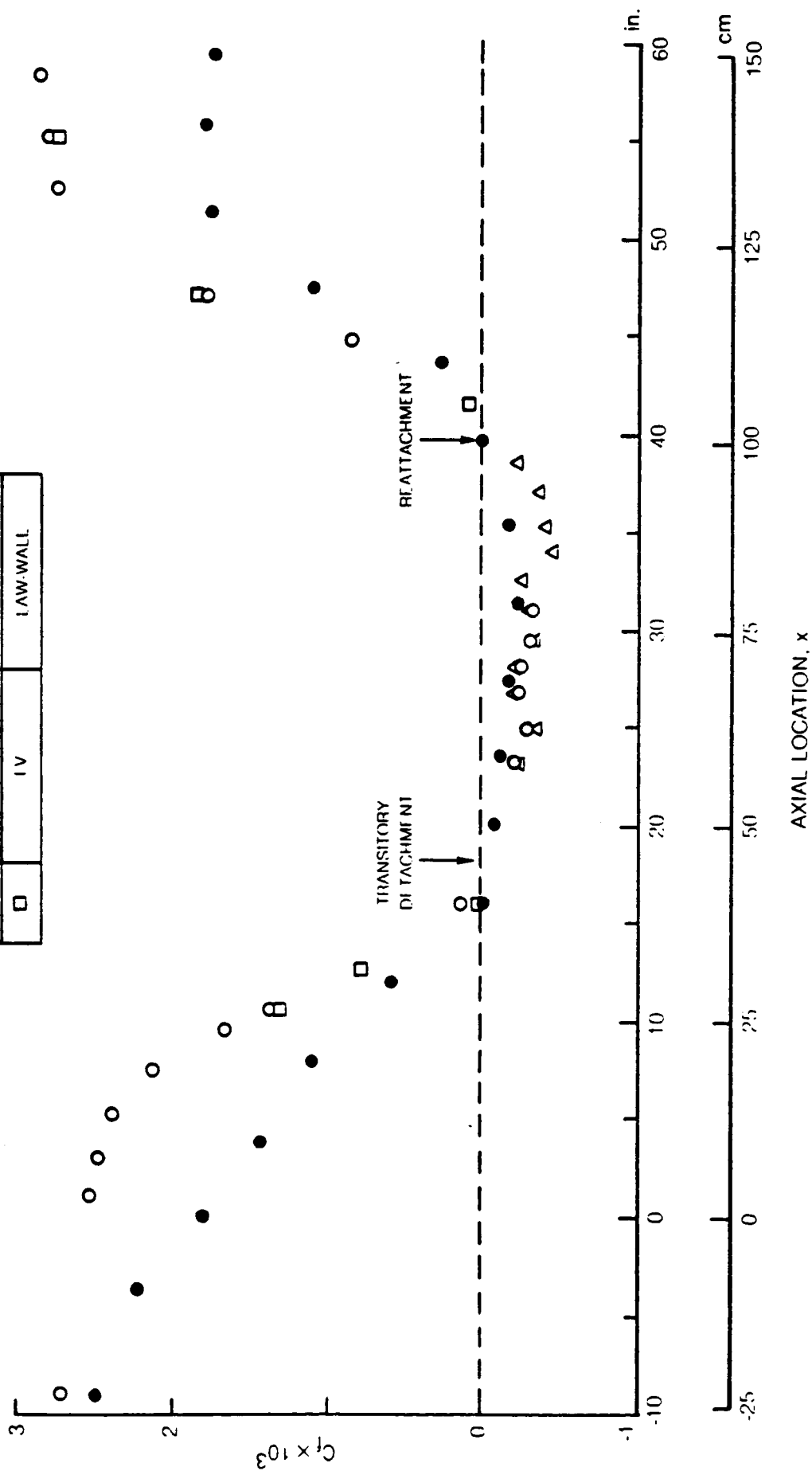
Fig. 4 Skin Friction Coefficient on Test Surface (z = 0, after Patrick [1]). Comparison of calculation results and measurements.

$P_{EXIT}/P_0 = 0.805$

$P_{EXIT}/P_0 = 0.722$

Fig. 5 SAJBEN TRANSONIC DIFFUSER STATIC PRESSURE, P/P_0, CONTOUR INTERVAL = 0.025
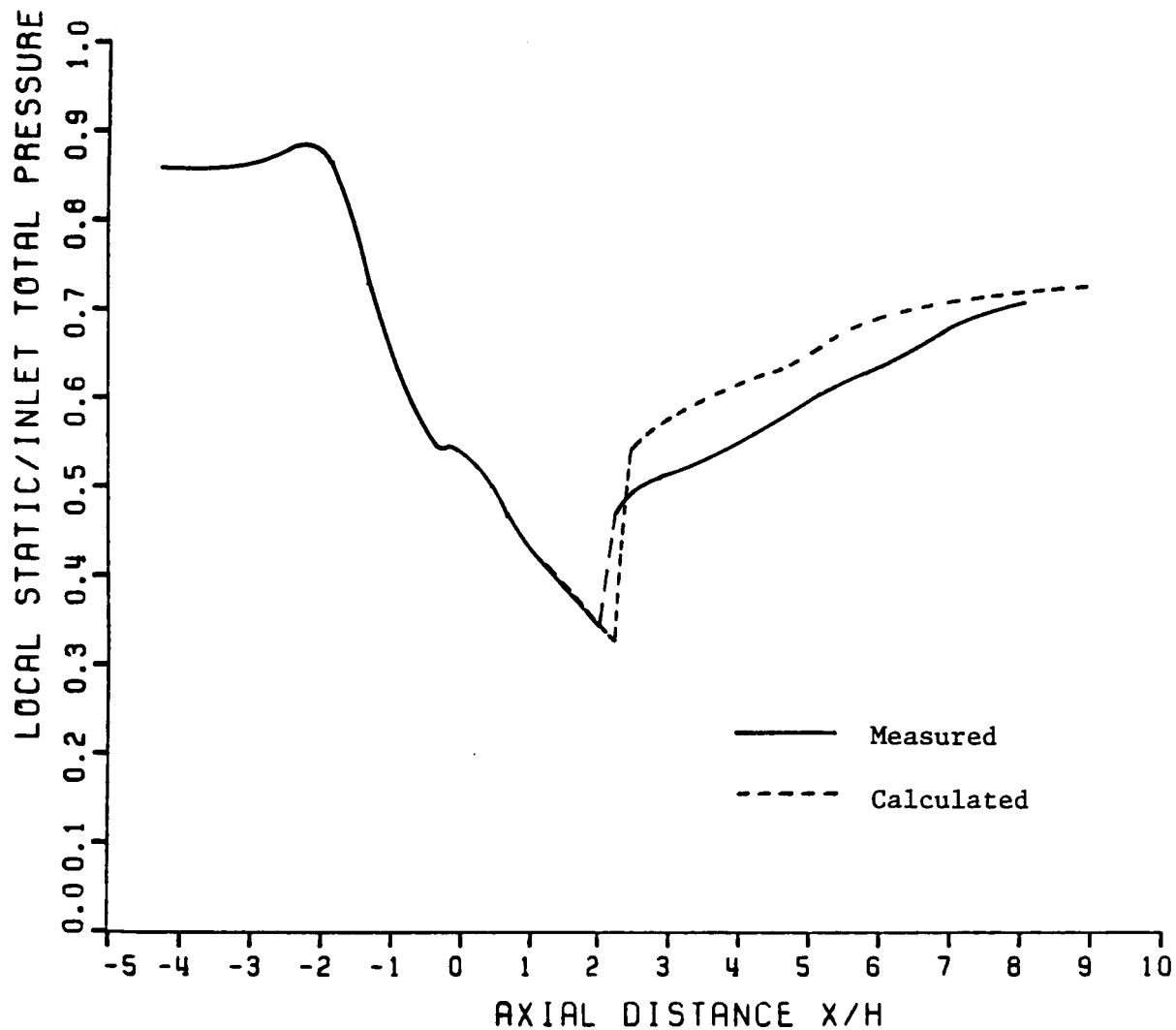
Fig. 6   Computed and measured static pressure distributions
on the curved top wall of the MDRL diffuser.
Strong shock case; $P_{exit}/P_{0inlet} = 0.722$.

$P_{EXIT}/P_0 = 0.805$

$P_{EXIT}/P_0 = 0.722$
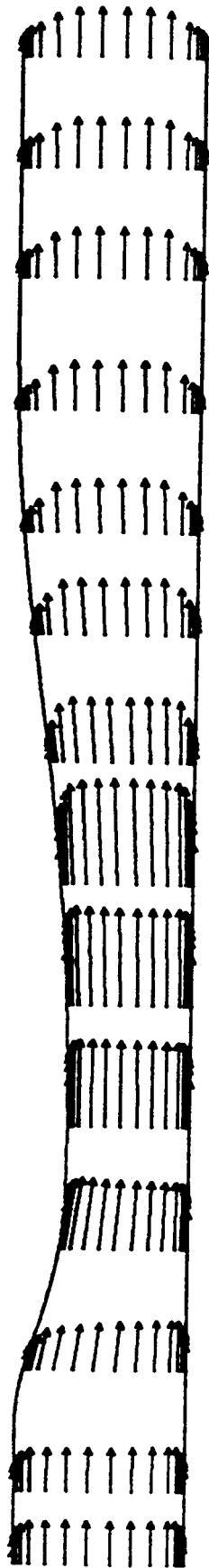
.5

.6

.5

.7

.8

1.2

1.2

.5

.5

Fig. 7 SAJBEN TRANSONIC DIFFUSER MACH NUMBER, CONTOUR INTERVAL = 0.05

$P_{EXIT}/P_0 = 0.805$

$P_{EXIT}/P_0 = 0.722$

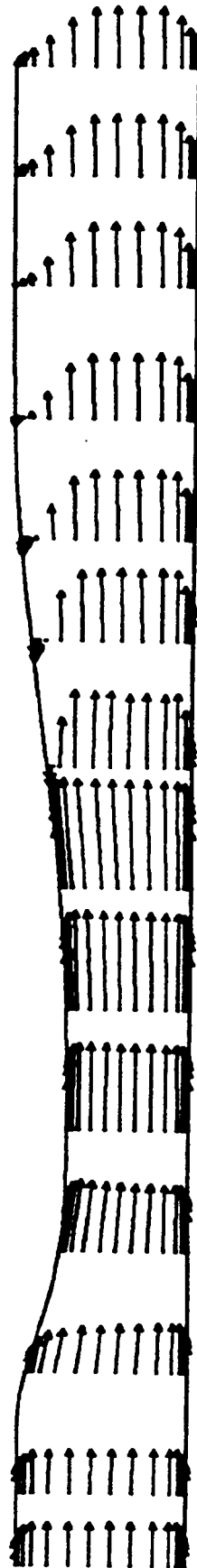Fig. 8   SAJBEN TRANSONIC DIFFUSER   CALCULATED VELOCITY VECTORS
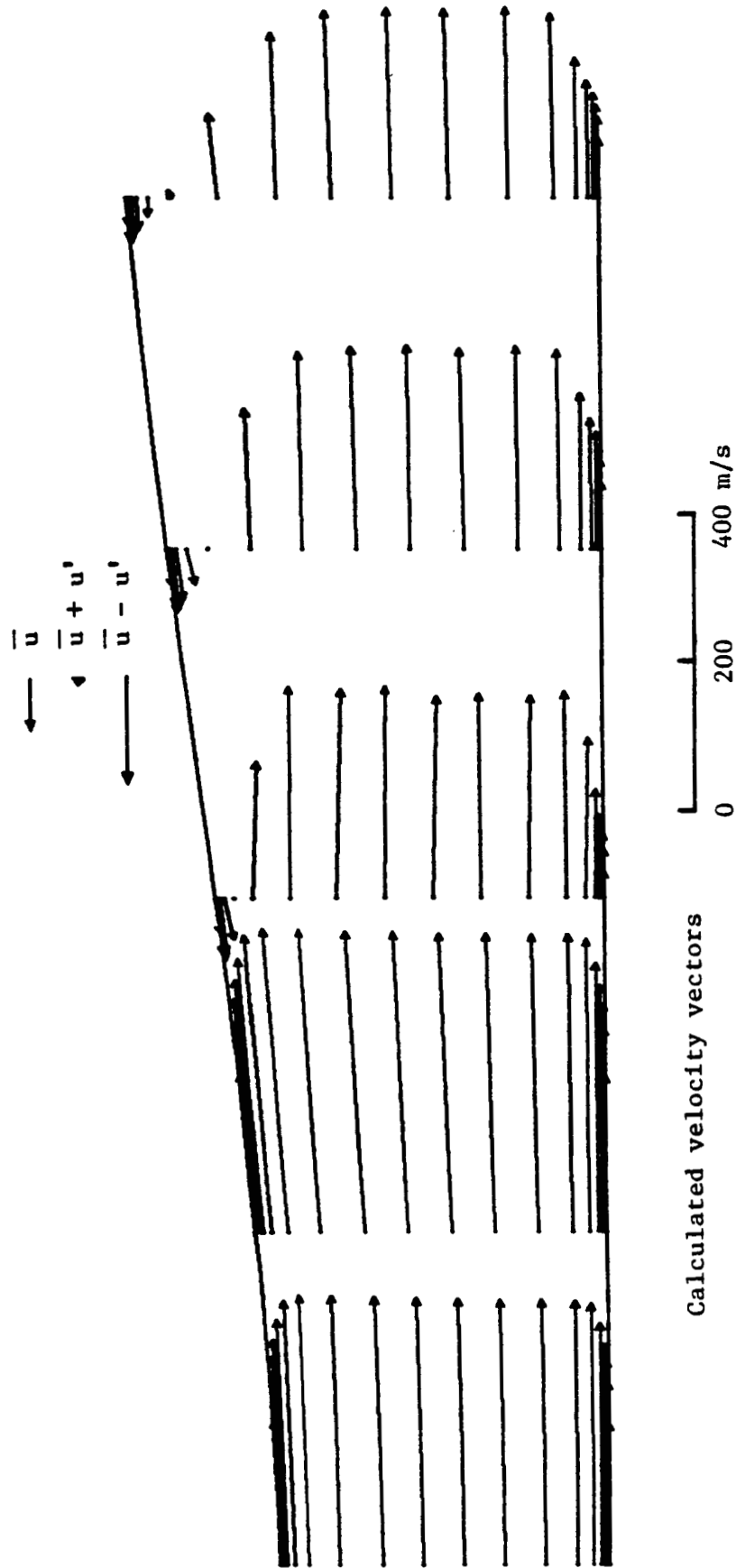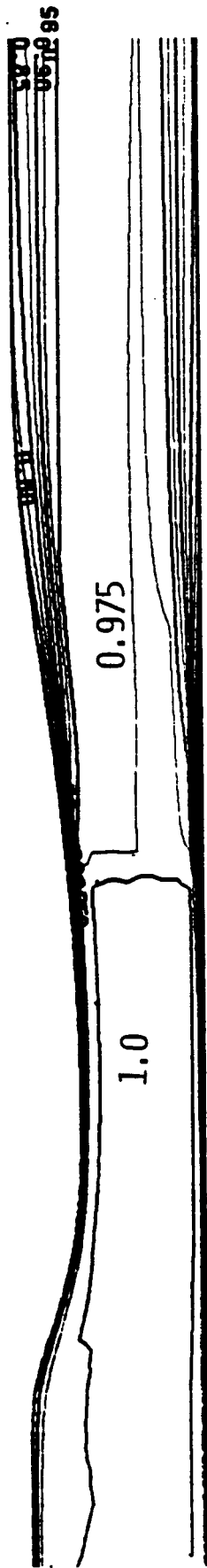
SAJBEN   PE/PO = 0.722

Largest Measured Backflow

$\overline{u}$

$\overline{u} + u'$

$\overline{u} - u'$

Calculated velocity vectors

0   200   400 m/s

Fig. 9   Calculated velocity vectors upstream of and within the separation bubble.

$P_{EXIT}/P_0 = 0.805$

0.975

1.0

$P_{EXIT}/P_0 = 0.722$

0.95

1.0

Fig. 10 SAJBEN TRANSONIC DIFFUSER Total Pressure, P_T/P_0, Contour Interval = 0.025

6. MACH NUMBER DEPENDENT INTERPOLATION FORMULA FOR DENSITY-UPDATE TIME-MARCHING METHODS

A 1-d stability analysis of density-pressure relations used in the computation of transonic flow was performed in Report No. JM/85-11 (see section 3 of this report, reference 3). Here we give a parallel development of a density interpolation equation for effective pressure for use in density-update methods. The formulae considered are tested using the density-update scheme outlined in Table 1.

Downwind Effective Pressure

In section 2.8 of reference 3, we considered an inconsistency in the pressure-density relation such that the pressure used in the momentum equation is offset by one grid point from the density used in the continuity equation, i.e.

$$P_i = \rho_{i+1} RT. \tag{40}$$

In a density update method this may be viewed as an effective pressure evaluated downwind of its point of use in the momentum equations. This pressure-density relation was found to be stable for all Mach numbers, but it results in poor shock capturing as the calculated shock is spread over numerous grid points. Fig. 1 shows the calculated and theoretical pressure distributions for a 1-d calculation with a nominal shock number of 1.45.

Mach Number Dependent Interpolation Formula for Effective Pressure

In section 2.6 of reference 3, we saw that when the Mach number is high, the density update method is stable with the ideal gas equation of state satisfied at each grid point, i.e.,

$$P_i = \rho_i RT_i \tag{73}$$

Since this is the correct pressure-density relation for ideal gases it should be used where feasible. In this section, we will start with a generalized density interpolation equation for effective pressure

$$\rho_i^e = \rho_{i+1} + a_0(\rho_i - \rho_{i+1}) + \frac{a_1}{2}(\rho_i - \rho_{i+2}) + \frac{a_2}{3}(\rho_i - \rho_{i+3}) \tag{74}$$

with
$$P_i = \rho^e_i RT_i \tag{75}$$

and
$$a_o + a_1 + a_2 = 1 \tag{76}$$

for second order accuracy.

We seek Mach number limitations to a_o, a_1 and a_2 using the stability criterion that

the center point coefficient must be greater than
the sum of the other positive coefficients,

$$\text{Coef}_{\text{center}} > \text{Sum Coef}_+ . \tag{46}$$

Substituting

$$\frac{\delta p_i}{RT} = (a_o + \frac{a_1}{2} + \frac{a_2}{3})\delta\rho_i + (1-a_o)\delta\rho_{i+1} - \frac{a_1}{2}\delta\rho_{i+2} - \frac{a_2}{3}\delta\rho_{i+3} \tag{77}$$

into Eq. 25 of reference 3 and rearranging in terms of the coefficients of each $\delta\rho_i$, a_0, a_1, and a_2, yields (neglecting variations of A, u and c with i)

$$\frac{Ac}{\gamma(M+1)} \{ (\qquad\qquad\qquad\qquad \tfrac{1}{3} a_2) \delta\rho_{i+4}$$

$$(\qquad\qquad\qquad \tfrac{1}{2} a_1 - \tfrac{2}{3} a_2) \delta\rho_{i+3}$$

$$(\quad -1 \quad\quad + a_o - \quad a_1 + \tfrac{1}{3} a_2) \delta\rho_{i+2}$$

$$(2+M\gamma(M+1) - 3a_o \qquad\quad - \tfrac{1}{3} a_2) \delta\rho_{i+1}$$

$$(-1-M\gamma(M+1) + 3a_o + \quad a_1 + \tfrac{2}{3} a_2) \delta\rho_i$$

$$(\qquad\qquad - a_o - \tfrac{1}{2} a_1 - \tfrac{1}{3} a_2) \delta\rho_{i-1} \}$$

$$= \dot{m}_{\text{change},i} . \tag{78}$$

Now let us consider a simple second order scheme with $a_2 = 0$ and $a_1 = 1 - a_0$, and find limiting values of a_o. From Eq. 74, it is obvious that we should consider only values in the range

$$0 \le a_o \le 1. \tag{79}$$

In this range, the coefficient of $\delta\rho_{i+3}$ is positive or zero, and for the coefficient of $\delta\rho_{i+1}$ (the center point) to be greater than the coeffcient of $\delta\rho_{i+3}$, we require

$$a_o < \frac{3}{5} + \frac{2}{5} M\gamma(M+1). \tag{80}$$

The coefficient of $\delta\rho_i$ is positive when

$$2a_o - M\gamma(M+1) > 0 \quad \text{or} \quad M(M+1) < 2a_o/\gamma. \tag{81}$$

In this region, from Eq. 46, we require

$$2 + M\gamma(M+1) - 3a_o > \frac{1}{2} - \frac{a_o}{2} + 2a_o - M\gamma(M+1) \tag{82}$$

or

$$a_o < \frac{1}{3} + \frac{4}{9} M\gamma(M+1) . \tag{83}$$

This criterion is more restrictive that Eq. 80 and the corresponding stability limit is shown as a function of Mach number in Fig. 2 for the conservative case of $\gamma = 1.0$.

A set of equations for a_o, a_1 and a_2, which satisfy the stability criteria (Eqs. 80 and 83) and give second order accurate interpolation (Eq. 76) has been selected; that is

$$a_o = \frac{4}{9} M(M+1)$$

$$a_1 = 1 - a_o \tag{84}$$

$$a_2 = 0.$$

This Mach number dependent formulation for a_o and a_1 is shown in Fig. 3. These equations are referred to as the M&M Mach number dependent interpolation formula for density-update time-marching methods.

Computational Tests of the M&M Density Interpolation Formula

In this section, results of shock capturing with the M&M formula (Eq. 84) in the density update method (Table 1) are presented for Denton's 1-d nozzle.

Calculation Details

Number of axial grid points = 46, δx = 1
At inlet   i = 1,   M = 0.80
For air   k = 1.4,   R = 287. J/kgK
$P_{exit}/P_{t,inlet}$ = 0.85, 0.80, 0.75

Results

The variations of static pressure, Mach number, and total pressure for all three back pressures are shown in Fig. 4. All three shocks are captured over four steps. The upstream side of the shock is sharply defined with only minor deviations from the theoretical 1-d solution. On the downstream side, there is a small overshoot and undershoot in static pressure and Mach number over two steps; the total pressure distributions show no overshoots or undershoots and show a sharp decrease over two steps.

Concluding Remarks

It is hoped that the M&M density interpolation formula will be useful to those organizations like NASA Lewis who are using density-update time-marching codes. It is also hoped that the stability analysis performed under this NASA Grant will be enlightening to users and developers of time-marching codes.

Table 1. Outline of Effective Pressure Method with Different Time Steps - Density Update Scheme.

UNKNOWNS (2 - DIMENSIONS)

$$\rho, u, v, (\rho u), (\rho v), (\rho e_o), h_o, P, T$$

CONTINUITY

$$\frac{\partial \rho}{\partial t} + \nabla \cdot (\rho \underline{u}) = 0 \qquad (1)$$

$$\delta \rho = (-\oint (\rho \underline{u}) \cdot d\underline{A}) \, \delta t_c / Vol$$

$$\rho = \rho + \delta \rho$$

$$P = \rho RT$$

MOMENTUM (INVISCID)

$$\frac{\partial}{\partial t}(\rho \underline{u}) + \nabla \cdot (\rho \underline{u}) \, \underline{u} = -\nabla p \qquad (2)$$

USING EQ. 2 - (u or v) TIMES EQ. 1

$$\rho \delta u = (-\oint (u(\rho \underline{u}) \cdot d\underline{A} + p \underline{i} \cdot d\underline{A})$$
$$+ u \oint (\rho \underline{u}) \cdot dA)) * \delta t_m / Vol$$

$$\rho \delta v = (-\oint (v(\rho \underline{u}) \cdot d\underline{A} + p \underline{i} \cdot d\underline{A})$$
$$+ v \oint (\rho \underline{u}) \cdot d\underline{A})) * \delta t_m / Vol$$

$$u = u + \delta u$$

$$v = v + \delta v$$

$$(\rho u) = \rho u$$

$$(\rho v) = \rho v$$

ENERGY

$$h_o = constant$$

$$T = (h_o - \frac{u^2 + v^2}{2})/C_p$$

DENTØN 1D EXAMPLE   AO= 0   A1= 0
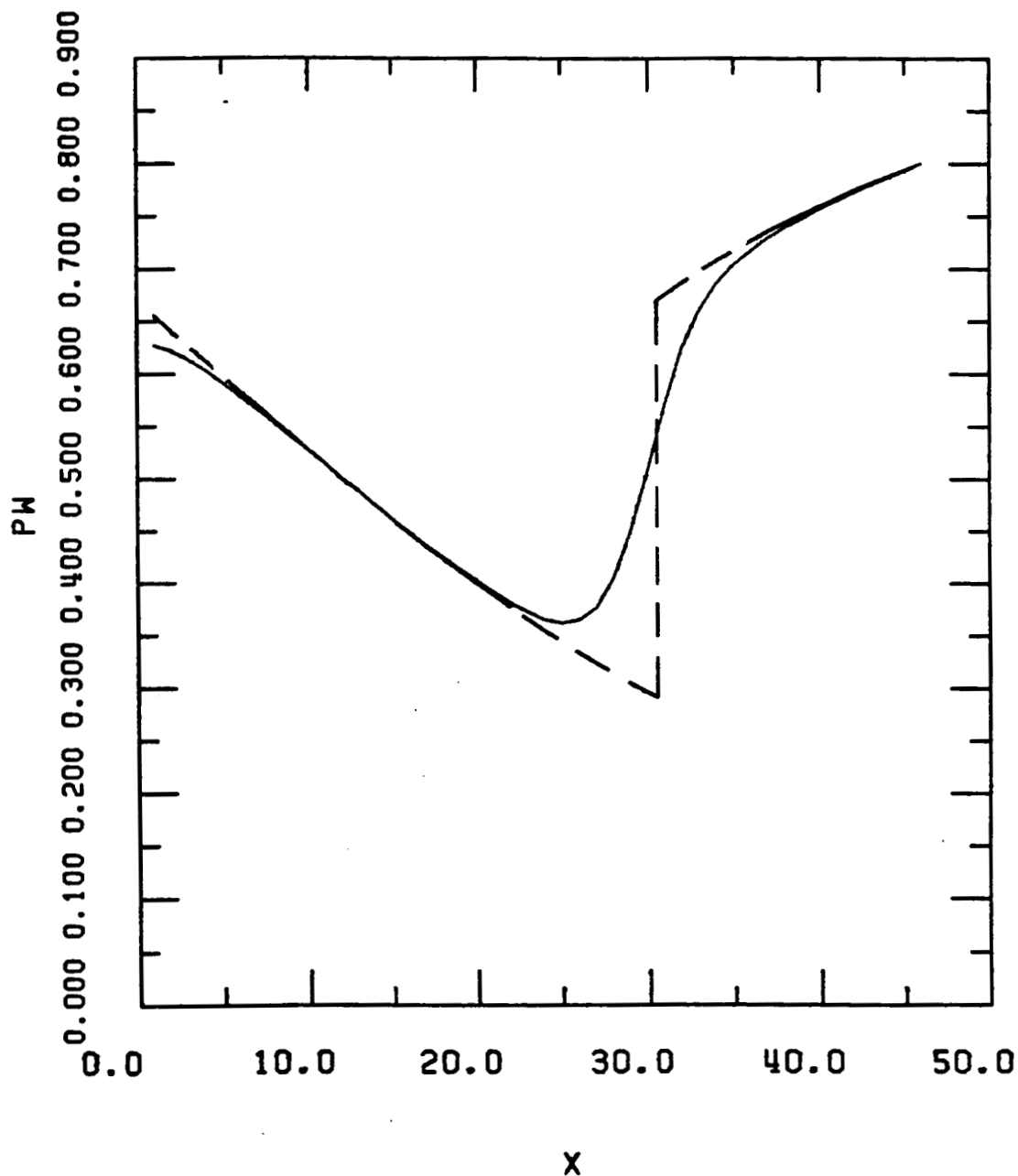

Fig. 1   Comparison of calculated and theoretical 1-D static

pressure distributions, PW = $P/P_{t,inlet}$.

————— ——— theoretical;

————————— calculated using a downwind effective pressure, Eq. 4

Grid spacing, $\delta x = 1$; $P_{exit}/P_{t,inlet} = 0.80$.
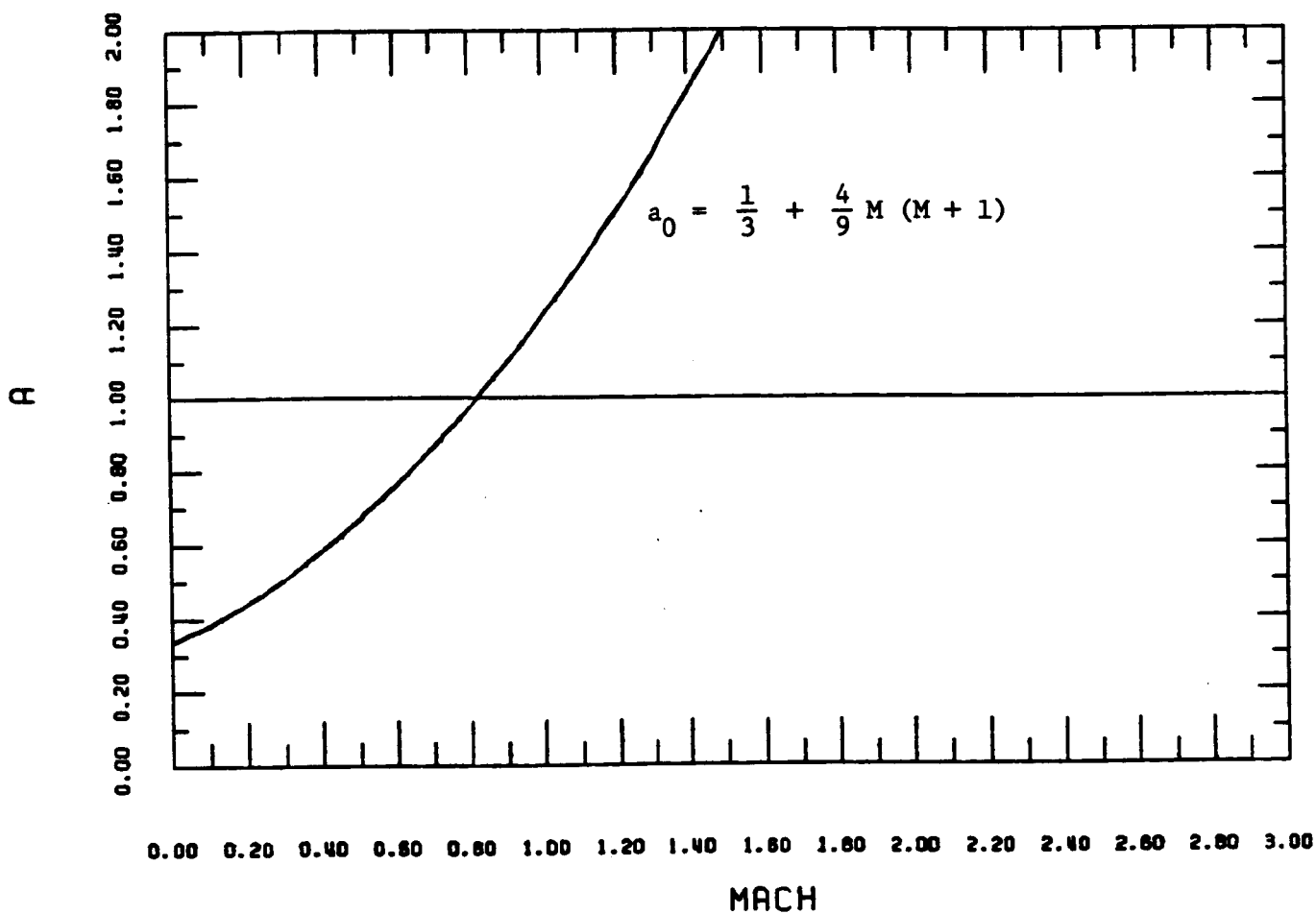
STABILITY LIMITS, A0+A1=1

$$a_0 = \frac{1}{3} + \frac{4}{9} M (M + 1)$$

Fig. 2   M & M density interpolation formula for use with
Effective Pressure, Density Update, Time Marching Methods.

Stability limits for a_0 when $a_2 = 0$ and $a_0 + a_1 = 1$.
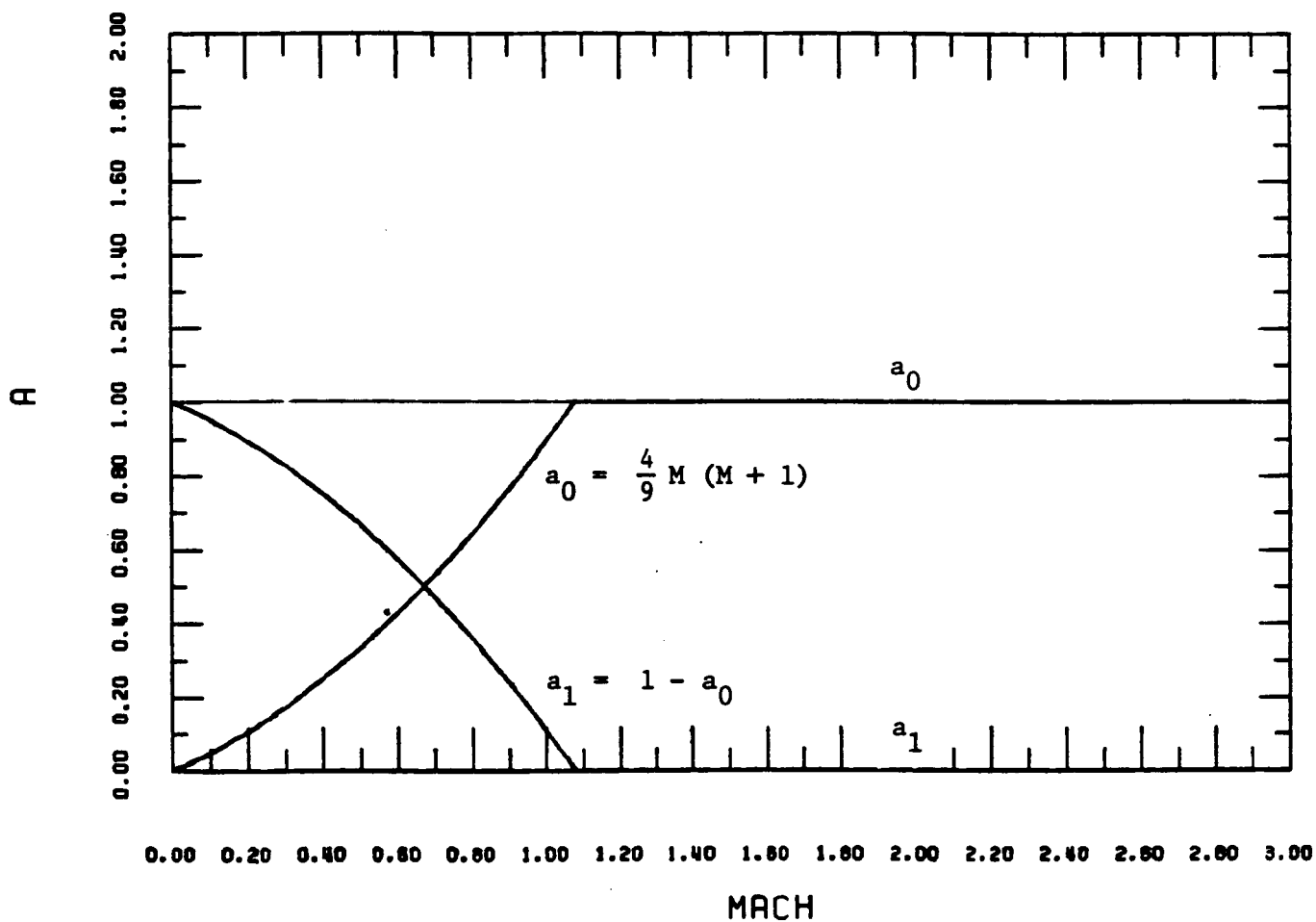
MACH NUMBER DEPENDENT A'S WITH A0+A1=1

$$a_0 = \frac{4}{9} M (M + 1)$$

$$a_1 = 1 - a_0$$

Fig. 3   M & M Mach number dependent values for the density interpolation
coefficients, a_0 and a_1, in the Effective Pressure Method.

DENTON 1D EXAMPLE   AO=M×(M+1)×4/9   A1=1-AO
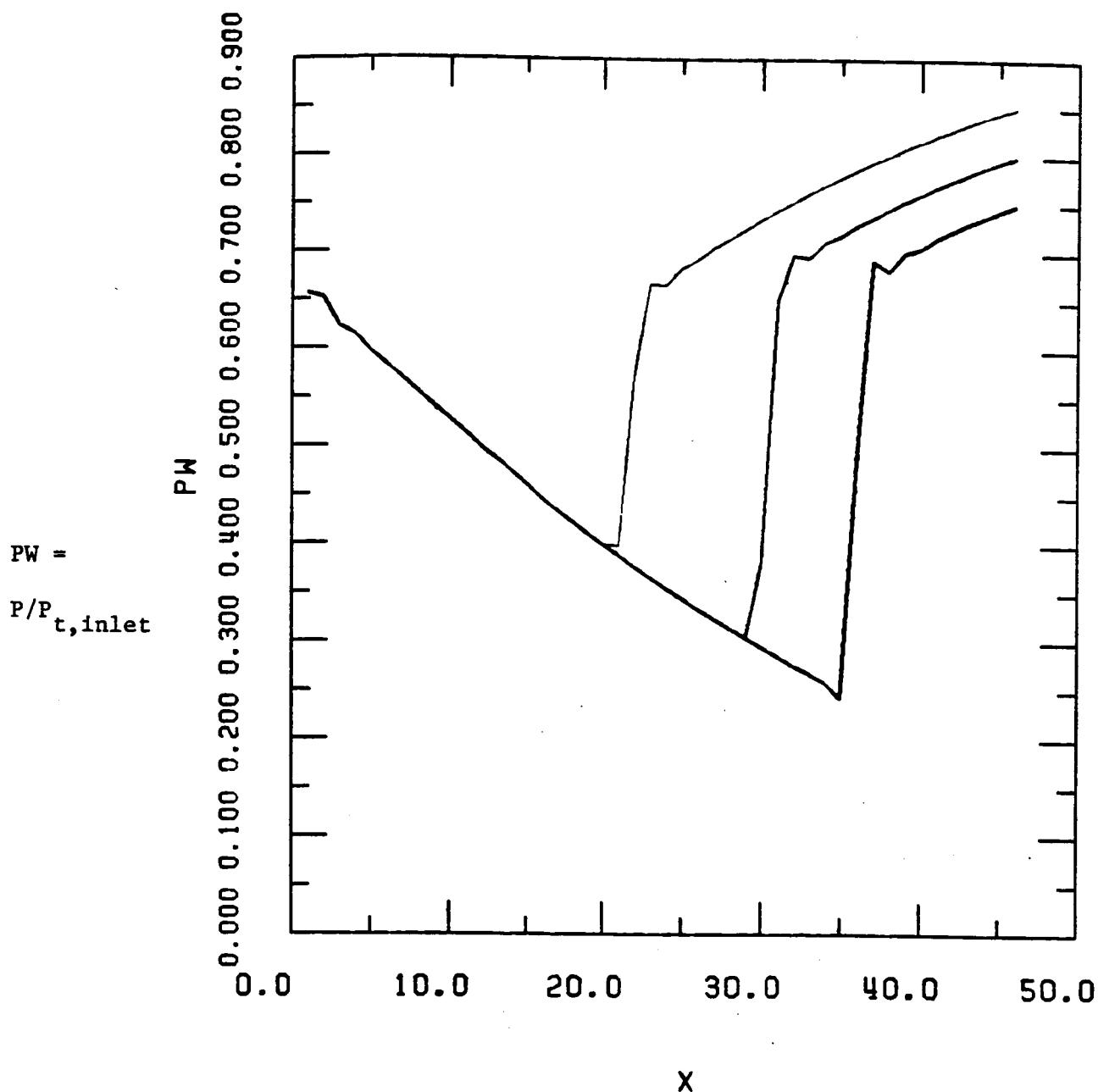
PW =

$P/P_{t,inlet}$

Fig. 4a   Calculated 1-D solution for Denton's nozzle
            using M & M density interpolation formula
            with the Nicholson/Moore Effective Pressure,
            Density Update Method.

            Calculations for three exit static pressures at x = 46.,
            $P_{exit}/P_{t,inlet}$ = 0.85, 0.80, and 0.75.

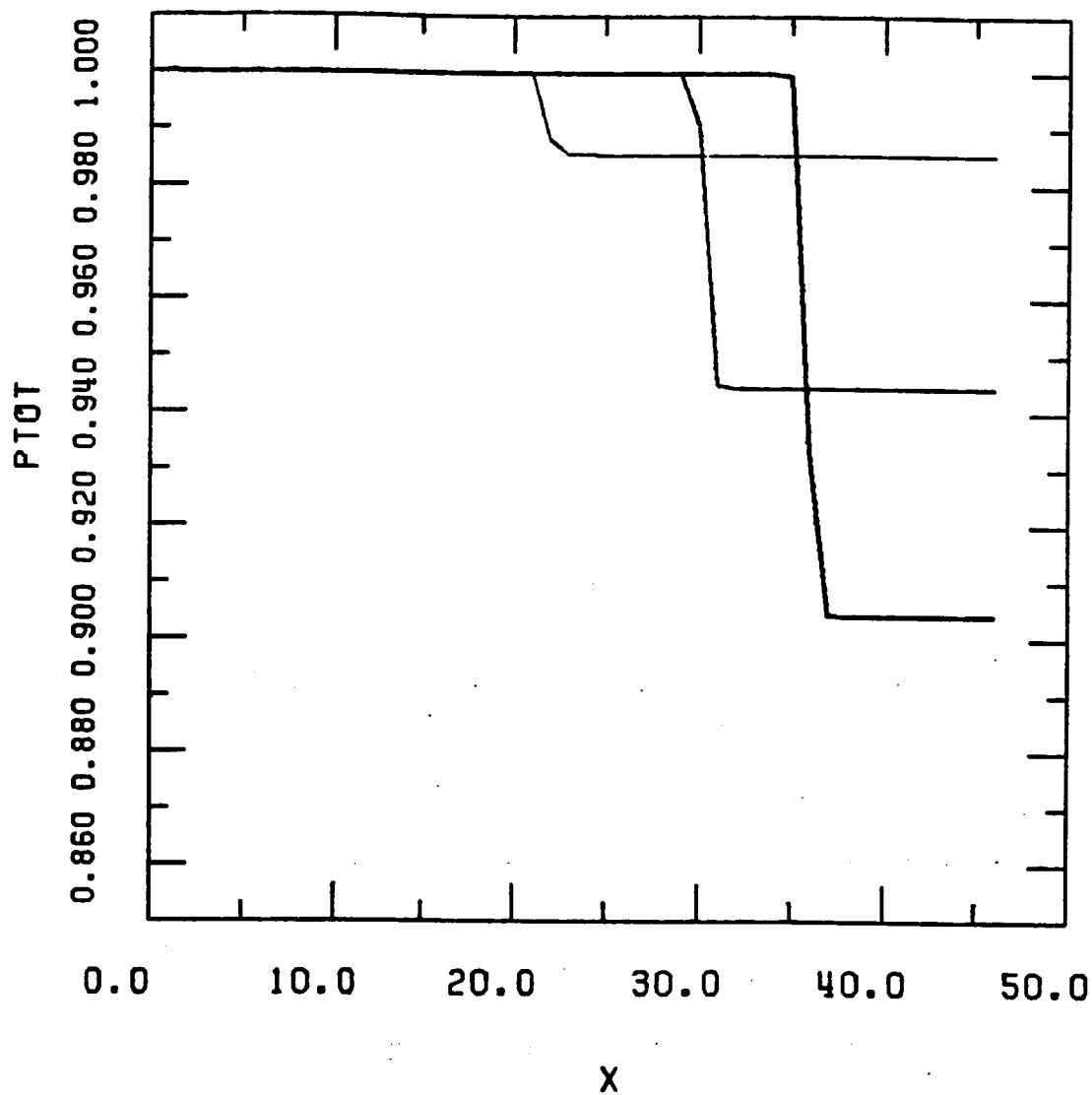DENTON 1D EXAMPLE   AO=M×(M+1)×4/9   A1=1−AO

Fig. 4b **Mach number.**

DENTON 1D EXAMPLE   A0=M×(M+1)×4/9   A1=1-A0

Fig. 4c PTOT = $P_t/P_{t,inlet}$.